Impact of proximity between NiMoS and zeolitic HY sites on cyclohexene hydroconversion: an infrared (IR) operando study of sulfide catalysts

Bruno M Santos, Weitao Zhao, José L Zotin, Mônica A.P. Da Silva, Laetitia Oliviero, Françoise Maugé

Impact of proximity between NiMoS and zeolitic HY sites on cyclohexene hydroconversion: an infrared (IR) operando study of sulfide catalysts

Bruno M. Santos*[1,2], Weitao Zhao[3], José L. Zotin[1],
Mônica A. P. da Silva[2], Laetitia Oliviero[3] and Françoise Maugé[3]

[1] *Centro de Pesquisas e Desenvolvimento, PETROBRAS, Rio de Janeiro (Brazil)*

[2] *Escola de Química, Centro de Tecnologia, Universidade Federal do Rio de Janeiro, Rio de Janeiro (Brazil)*

[3] *Normandie Univ, ENSICAEN, UNICAEN, CNRS, LCS, 14000 Caen (France)*

*bruno_m@petrobras.com.br

Abstract

This work evaluates the effects of sulfide phase location on zeolite-containing catalysts on cyclohexene hydroconversion using the infrared (IR) operando technique. Parallels between activity, product yield, and surface species changes with time-on-stream and by pyridine poisoning were performed on pure HY zeolite, sulfided NiMo/HY, NiMo/Al_2O_3, and NiMo/Al_2O_3+HY. Isomerization activity could be related to zeolitic acidic OH groups and hydrogenation activity to sulfide phase sites. From the changes due to pyridine pulse injection, intrinsic activities could be calculated for isomerization (1-methyl-1-cyclopentene) and hydrogenation (cyclohexane) routes. The turnover frequency (TOF) value for isomerization is greater by one order of magnitude than that for hydrogenation. Hence, the poisoning effect of one N-molecule will be 10 times higher on isomerization than on the hydrogenation route. Whatever the location of the sulfide phase, the coke is mostly formed on the zeolite. As a

consequence on NiMo/HY, the close proximity between acidic and sulfide sites results in lower formation of hydrogenated products due to blockage of some sulfide sites by coke. In contrast, hydrogenation activity of NiMo/Al_2O_3 + HY is less affected by coke, NiMoS being mostly located on alumina. However, the results show that the close proximity between acid and sulfide sites allows a higher degree of hydrogenation of the isomerization product (1-methyl-1-cyclopentene). Thus, the higher proximity has a beneficial effect on methylcyclopentane formation.

Keywords: cyclohexene, operando, sulfides, NiMo, zeolite, Infrared (IR) spectroscopy

Graphical abstract

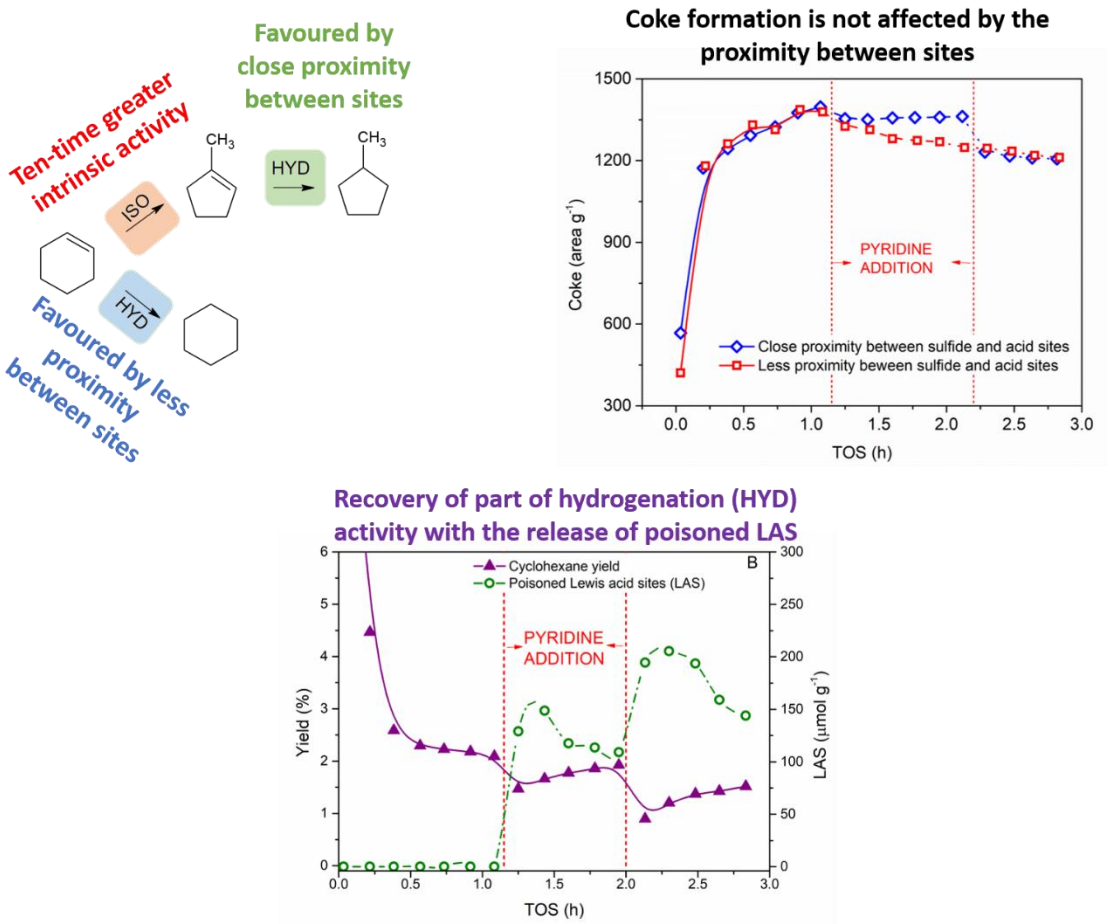

1. Introduction

Diesel specification has become stricter along the years, especially in terms of density and cetane number. Thus, hydrogenation of aromatic compounds followed by ring-opening of the naphthenic cycle has been extensively investigated in the literature to improve fuel quality. Such studies are carried out on bifunctional catalysts, where hydrogenation/dehydrogenation (metal or sulfide sites) and acid functions (zeolites, responsible for isomerization and cracking steps) are evaluated [1–4]. In this context, there are key parameters that interfere in this selectivity, such as the balance between acidic and hydrogenation functions, nature and acidic strength of acid support, diffusion of formed products, among others [1,3,5]. The proximity between these sites is reported as a positive factor for improving ring-opening reactions and minimizing cracking due to shorter diffusion distances [3,6]. On the other hand, the presence of nitrogen compounds in hydroprocessing feedstocks is a common source of catalyst deactivation [7–9]. These compounds are strongly adsorbed on the catalyst, neutralizing Brønsted acid sites of zeolite and reducing catalytic activity.

Operando infrared (IR) spectroscopy is a technique that allows the monitoring of the catalyst surface sites during the reaction under working conditions [10]. In the last decade, many studies based on operando IR spectroscopy were published [10–14], but very few papers report investigations of sulfide catalysts [8,15]. However, the investigation of the role of active sites by operando IR spectroscopy may provide valuable information about these bifunctional materials. This study focuses on cyclohexene hydroconversion. Indeed, cyclohexene is a suitable reactant for such studies because it is an intermediate for isomerization and hydrogenation reactions and such molecule is easily converted at conditions allowed by the infrared operando setup [16], such as atmospheric pressure and appropriate temperature. The reaction scheme for cyclohexene transformation is widely known [10,17–25] and shown in Figure 1. Three routes are possible: dehydrogenation to benzene, hydrogenation to cyclohexane, or isomerization to 1-methyl-1-

cyclopentene, which can be further hydrogenated to methylcyclopentane. ~~However, the implication of the various sites of the catalyst in these various routes is still questionable.~~

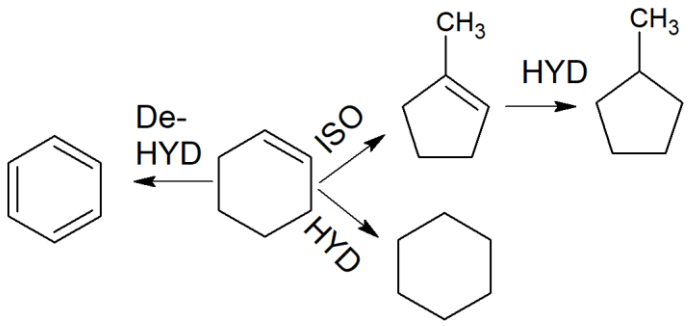

Figure 1. Cyclohexene hydroconversion scheme. De-HYD: dehydrogenation; HYD: hydrogenation; ISO: isomerization.

Thus, this work aims to investigate, by FTIR operando study, the effects of proximity between sulfide and acid sites on cyclohexene hydroconversion. This study will contribute to understanding how the location of sulfide sites affects coke formation, as well as the influence of nitrogen compounds (pyridine) on the activity and selectivity of catalysts regarding isomerization and hydrogenation reactions.

2. Materials and Methods

2.1 Catalyst Preparation

NiMo catalysts were synthesized using two supports: alumina (Pural SB, SASOL) and HY zeolite (Zeolyst Inc, Si/Al mol ratio = 15, framework Si/Al = 25). The catalyst supported on alumina (Alu) was prepared by a previously described procedure [4]. The impregnation solution was prepared by solubilization of 2.1 g of ammonium heptamolybdate (99%, VETEC), followed by dissolution of 1.3 g of nickel nitrate hexahydrate [Ni $(NO_3)_2.6H_2O$] (97%, VETEC) in perydrol solution (30%wt.) to a final volume of 17 mL. The pH of the solution was adjusted

to 2.5 by addition of concentrated ammonium hydroxide. This solution was added to 15 g of alumina support (wetness impregnation), followed by manual homogenization for 1 hour. The catalyst was dried at 473 K for 1 hour and then calcined at 723 K for 1 hour, with a heating rate of 10 K min^{-1}. The expected contents are 2 wt.% of NiO and 10 wt.% of MoO_3, and it was identified as NiMo/Alu. The catalyst supported on HY zeolite was prepared by previous addition of Ni by three steps of ionic exchange with a 0.1 mol L^{-1} nickel nitrate hexahydrate solution [Ni $(NO_3)_2.6H_2O$] (97%, VETEC) at 343 K, followed by drying at 473 K for 2 hours and then calcining at 823 K for 2 hours. Mo was incorporated by a physical mixture between 20 g of Ni-exchanged zeolite and 2.2 g of MoO_3 (99.9%, Molymet), followed by manual grinding for 5 minutes and thermal treating at 723 K for 24 hours. The expected content of this catalyst is 2 wt.% of NiO and 10 wt.% of MoO_3, and its identification was NiMo/HY. In the third catalyst, metals were firstly impregnated onto alumina, as described for NiMo/Alu preparation. Then, the obtained material was physically mixed with HY zeolite to contain 1.2 wt.% of NiO, 6.3 wt.% of MoO_3, 47.0 wt.% of zeolite and 45.5 wt.% of alumina, which was identified as NiMo/Alu+HY. For operando tests, NiMo/HY and NiMo/Alu+HY catalysts were compared either at the same metal or zeolite amounts by using a different mass of catalyst during their tests.

2.2 Catalyst characterization

NiO and MoO_3 content in the catalysts were determined by X-ray fluorescence (XRF), in a Panalytical equipment, model Magix Pro. The crystalline structure of supports and catalysts was measured by X-ray diffraction (XRD) in a Philips equipment, model PW1710, using CuKα radiation filtered by a monochromator at 40 kV and 55 mA, with scanning angle (2Θ) between 5 and 70° and velocity of 5° per minute. Textural properties of supports and catalysts were characterized by nitrogen adsorption at 77 K in a Tristar 3000 equipment from Micromeritics. Samples were submitted to an treatment at 723 K for 3 h and subsequently at 573 K for 1 h

under vacuum (50 mtorr) prior to analysis. Micropore properties were obtained by *t-plot* method for HY and NiMo/HY, while textural properties for Al_2O_3 and NiMo/Alu were determined by BET method. For NiMo/Alu+HY, such properties were evaluated by both methods. All results were normalized to the support content in each catalyst.

FTIR spectroscopy of adsorbed CO was used to characterize the sulfide phase. Samples were pressed into self-supported wafers (approximately 8 mg cm^{-2}) and dried *in situ* under vacuum overnight. Sulfidation was performed at 623 K for 2 h, under 30 mL min^{-1} of 10% H_2S in H_2 and heating rate of 3 K min^{-1}. After that, the catalyst was flushed with Ar for 0.25 h, kept under vacuum for 1 h at 623 K and then cooled to 298 K. CO adsorption was performed at low temperature (77 K), achieved with liquid nitrogen. Adsorption was carried out by introduction of small doses of CO up to an equilibrium pressure of 133 Pa. Spectra were scanned using a Nicolet spectrometer (Nexus) equipped with an MCT detector with 256 scans and 4 cm^{-1} resolution. All spectra were normalized to a sample disk of 500 mg cm^{-2}, and their decompositions were performed by OMNIC 9 peak fit, using Voigt fit analysis. Such spectra were taken after equilibrium at 133 Pa of CO.

2.3 Operando study

Samples were pressed into self-supported wafers with approximately 8 mg cm^{-2} and inserted in an operando FTIR cell previously described [10,26]. Before the tests, the catalysts were sulfided at 623 K for 2 h, at heating rate of 3 K.min^{-1}, and 30 mL min^{-1} of 10% H_2S in H_2. After, catalysts were kept at 623 K for 30 minutes at 30 mL min^{-1} of N_2, and then the temperature was decreased to 523 K at a rate of 3 K min^{-1}, when a flow of the reaction gas, composed of 1.0% of cyclohexene, 50% of H_2 and 49% of N_2 on a molar basis, was admitted into the system. Catalytic tests were carried out at 523 K, H_2/cyclohexene ratio of 50 mol/mol and cyclohexene WHSV of 5 h^{-1}. The composition of reactor effluent was determined by gas chromatography

(GC) and used to monitoring conversion and product yield, utilizing a Bruker 450-GC equipment, equipped with a column BP1 50 m x 0.32 mm and FID detector. Fourier Transform Infrared (FTIR) spectra, used to monitor the catalyst surface, were recorded on a Nicolet 6700 equipped with an MCT detector with 64 scans and 4 cm^{-1} resolution. After approximately 1 h of reaction, a pulse of pyridine (2.1 µmol) was added to the feed, and IR bands quantified poisoned Brønsted (BAS) and Lewis acid sites (LAS) at 1542 and 1450 cm^{-1}, using molar absorption coefficients (ε) of 1.8 µmol cm^{-1} [27] and 1.5 µmol cm^{-1} [28], respectively. After approximately 2 h of reaction, an additional dose of 2.1 µmol of pyridine was introduced to the system, and catalytic behavior was monitored by GC and IR, and poisoned BAS and LAS were quantified as described above.

3. Results and Discussion

3.1 Compositional, structural, and textural properties

Elemental analysis and textural properties of supports and catalysts are summarized in Table 1. NiO and MoO_3 contents exhibit close values to the theoretical ones. Textural characterization indicates that the specific area of NiMo/Alu is similar to the original support (Alu), considering the intrinsic analysis error (approximately 10%) [29]. On the other hand, NiMo/HY catalyst presents a decrease of micropore area compared to the pure zeolite. Textural properties of NiMo/Alu+HY are complicated to interpret due to the difficulty of isolating the contributions of zeolite and alumina, except for the micropore area, which can be exclusively attributed to the zeolite. In contrast to NiMo/HY, NiMo/Alu+HY exhibits a comparable micropore area to the pure zeolite~~, suggesting that the NiMo phase is preferentially deposited on alumina~~. Additionally, all zeolite-containing samples present analogous micropore volume, considering the intrinsic analysis error, in agreement with reported by previous works [30,31].

Table 1. Elemental analysis and textural properties

Samples	HY	Alu	NiMo/HY	NiMo/ Alu	NiMo/Alu+HY
NiO (wt.%)	-	-	1.7	2.2	1.3
MoO_3 (wt.%)	-	-	9.6	11.9	7.1
BET Area[b] (m^2 g^{-1})	771	244	665	271	504
Micropore area[a] (m^2 g^{-1})	547	-	458	13	591
External area[b] (m^2 g^{-1})	224	244	207	258	203
Pore volume[b] (cm^3 g^{-1})	0.19	0.48	0.20	0.45	0.30
Micropore volume[a] (cm^3 g^{-1})	0.25	-	0.26	-	0.28

[a] Normalized to alumina content on NiMo/Alu catalyst and zeolite content in NiMo/HY and NiMo/Alu+HY catalysts

[b] Normalized to support content on the catalyst ("HY+Alu" in NiMo/Alu+HY, "HY" in NiMo/HY and "Alu" in NiMo/Alu)

Pore size distributions and isotherms of the samples are exhibited in Figure 2. HY and NiMo/HY show a peak with a maximum at approximately 37 Å (Figure 2A) while Alu and NiMo/Alu exhibit a peak with maximum at 65 Å and NiMo/Alu+HY exhibit a combination of both peaks. For comparison reasons, an Alu+HY pore size distribution was created by a combination of Alu and HY distributions, properly normalized by the amount of each compound in the support. Then, the ratio between the dV/dlogD values at 65 Å (alumina contribution) and 37 Å (zeolite contribution) on Alu+HY and NiMo/Alu+HY was calculated, and the values obtained were 1.77 and 1.36, respectively, indicating that metals addition caused more impact on alumina distribution than the zeolite on NiMo/Alu+HY. Figure 2B shows the isotherms of the materials. HY and NiMo/HY exhibit similar isotherm profile and one can note a shift at p/p° close to 1 on NiMo/HY isotherm. Alu and NiMo/Alu also have similar profiles, with Alu exhibiting a shift at p/p° close to 1. NiMo/Alu+HY exhibit a combination of both isotherms and do not present a shift at higher p/p° values, as observed on NiMo/Alu. Thus, the comparable micropore area to the pure zeolite shown in Table 1, the lower ratio between alumina and zeolite contributions on pore distribution and the absence of shift on the isotherm at

higher p/p° values exhibited by NiMo/Alu+HY suggest that NiMo phase is preferentially deposed on alumina.

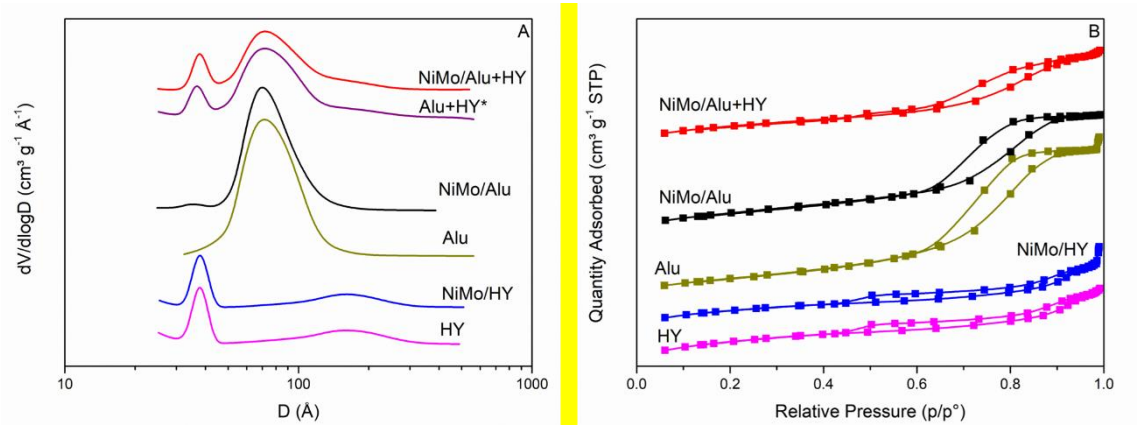

Figure 2. (A) Pore size distributions and (B) isotherms of the samples. *Pore size distribution of NiMo/Alu+HY was estimated by HY and Alu distributions, normalized by each compound content on the support.

X-ray diffractograms, illustrated in Figure 3, exhibit similar patterns between the catalysts and their respective supports. The absence of peaks related to MoO_3 aggregates (dashed lines) in the catalysts suggests suitable dispersion of metal species on the supports.

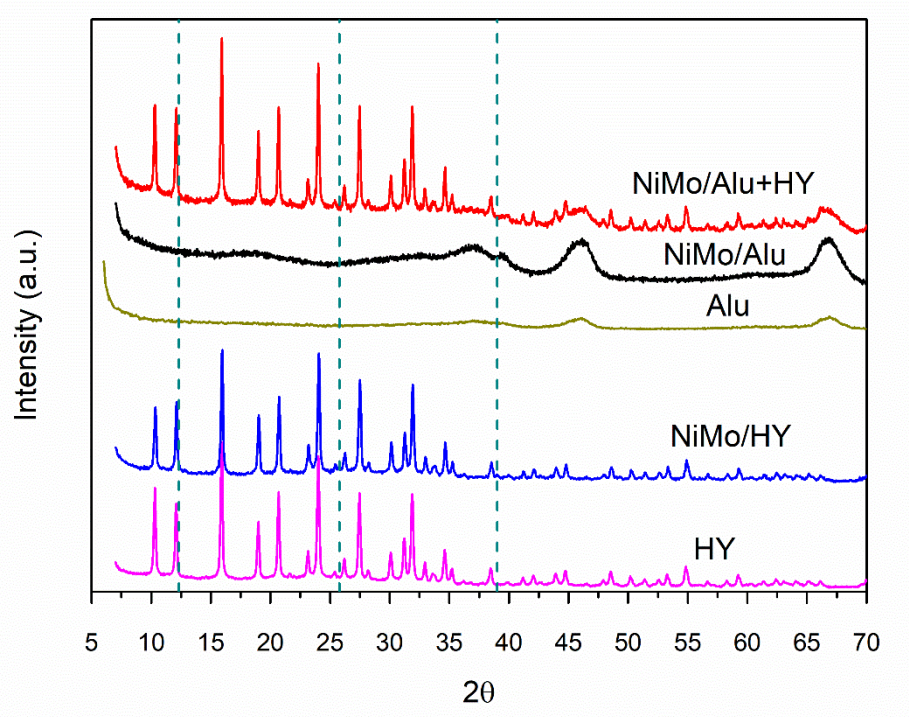

Figure 3. X-ray diffractograms of supports and catalysts. Dashed lines: MoO_3 diffraction peaks (JCPDS n° 05-0508)

3.2 Nature and location of sulfide sites

IR Spectra of CO adsorbed on the sulfide catalysts are presented in Figure 4A. Bands associated to CO interactions with the support are found between 2140 and 2190 cm^{-1} [32,33], while bands characterizing sulfide phase are observed below 2140 cm^{-1}. The CO spectra decomposition is presented in Figures S1 to S3. Wavenumbers of the sulfide phase sites are reported in Figure 4B. On NiMo/Alu, CO bands are observed at 2120-2124 cm^{-1} (promoted sites – Ni centers), 2107 cm^{-1} (unpromoted Mo sites), 2074-2079 cm^{-1} and 2040-2044 cm^{-1} (promoted sites – Mo centers) [33–35]. Previous works show that CO adsorbed frequencies on the sulfide phase strongly depend on support acidity [32,34,36,37]. On strong acidic zeolites such as Hβ, Mo sites are characterized by a band at 2131 cm^{-1} [32]. Thus, on NiMo/HY (Si/Al=15), the band at 2120 cm^{-1} is assigned to unpromoted Mo sites [38] in agreement with the lower acidic OH groups

than Hβ, although stronger acidic than alumina. Figure 4B shows that wavenumbers are always greater for each type of sulfide phase site when it is deposited on zeolite than on alumina. Note that the differences of wavenumbers raise (from 7 to 30 cm^{-1}) when the frequency decreases i.e. when the extent of the backdonation from sulfide sites to CO molecule increases. Interestingly, Figure 4B points out the closeness between the frequencies of sulfide sites of NiMo/Alu and NiMo/Alu+HY. Besides, Ni-promoted site proportion is greater on NiMo/HY catalysts than on alumina containing catalysts (Table S1). These behaviors evidence that on NiMo/Alu+HY, the sulfide phase is mostly in interaction with alumina, in agreement with the textural observations. This location should lead to a lower proximity between sulfide sites and BAS on NiMo/Alu+HY than on NiMo/HY catalysts.

Figure 4C exhibits IR spectra of OH groups after sulfidation. HY presents 3 clear OH bands. The first one, at 3740 cm^{-1}, is ascribed to silanol groups [39]. The second one, at 3633 cm^{-1}, is assigned to high-frequency OH groups (perturbed and non-perturbed by extraframework Al species), located in supercages [27,40,41] and the last one, at 3567 cm^{-1}, is associated with low-frequency OH groups, located in sodalite cages (perturbed and non-perturbed by extraframework Al species) and hexagonal prisms [35,41,42]. Nevertheless, the addition of Ni and Mo makes more significant the IR absorbance of the samples and thus strongly decreases the signal to noise ratio in the OH zone. Moreover, Ni and Mo can also interact with the support OH groups. This makes the OH bands weaker on NiMo/HY and NiMo/Alu+HY or even unobservable on NiMo/Alu.

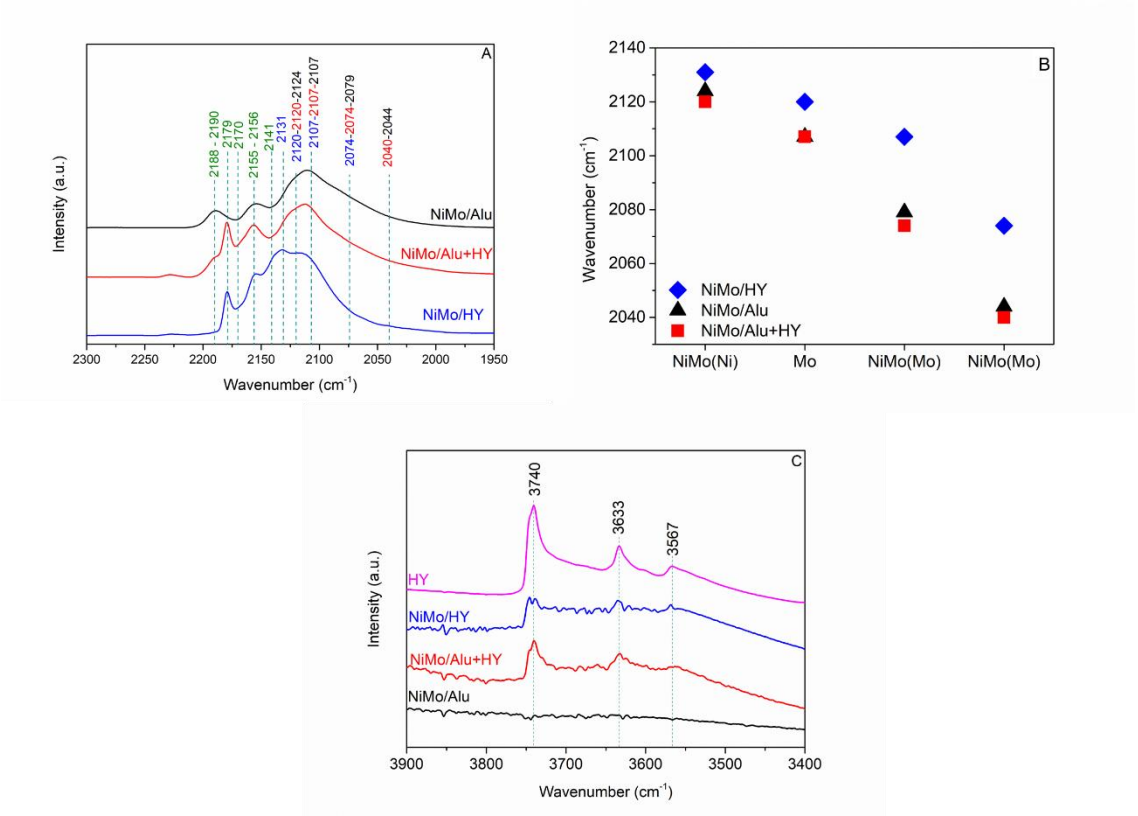

Figure 4. (A) IR Spectra of CO uptake (133 Pa, 100K) per gram of catalyst on the sulfide catalysts. Wavenumbers in green: CO interactions with support. Wavenumbers in blue, red and black: CO interactions with sulfide phase on NiMo/HY, NiMo/Alu+HY and NiMo/Alu, respectively. (B) Wavenumbers of the CO bands of the different sulfide phase components. (C) IR spectra of OH groups, normalized per gram of catalyst, after sulfidation.

3.3 Operando study

Operando infrared / gas chromatography (IR/GC) study simultaneously accounts for the surface species of the sulfide catalyst as well as for its cyclohexene conversion and product selectivity versus time-on-stream (TOS). After 10 minutes of reaction (Figure 5A), IR spectra present different bands relative to coke formation at ~1591, 1378, and 1348 cm^{-1}. In addition, a band at 1497 cm^{-1} observed on zeolite-containing catalysts and one at 1486 cm^{-1} on NiMo/Alu are assigned to unsaturated carbenium ions [9,10,43]. The band at about 1451 cm^{-1} is referred to as a

combination of adsorbed intermediate species and coke [9,10]. NiMo/Alu also exhibits additional bands at 1446 and 1455 cm^{-1} in this region.

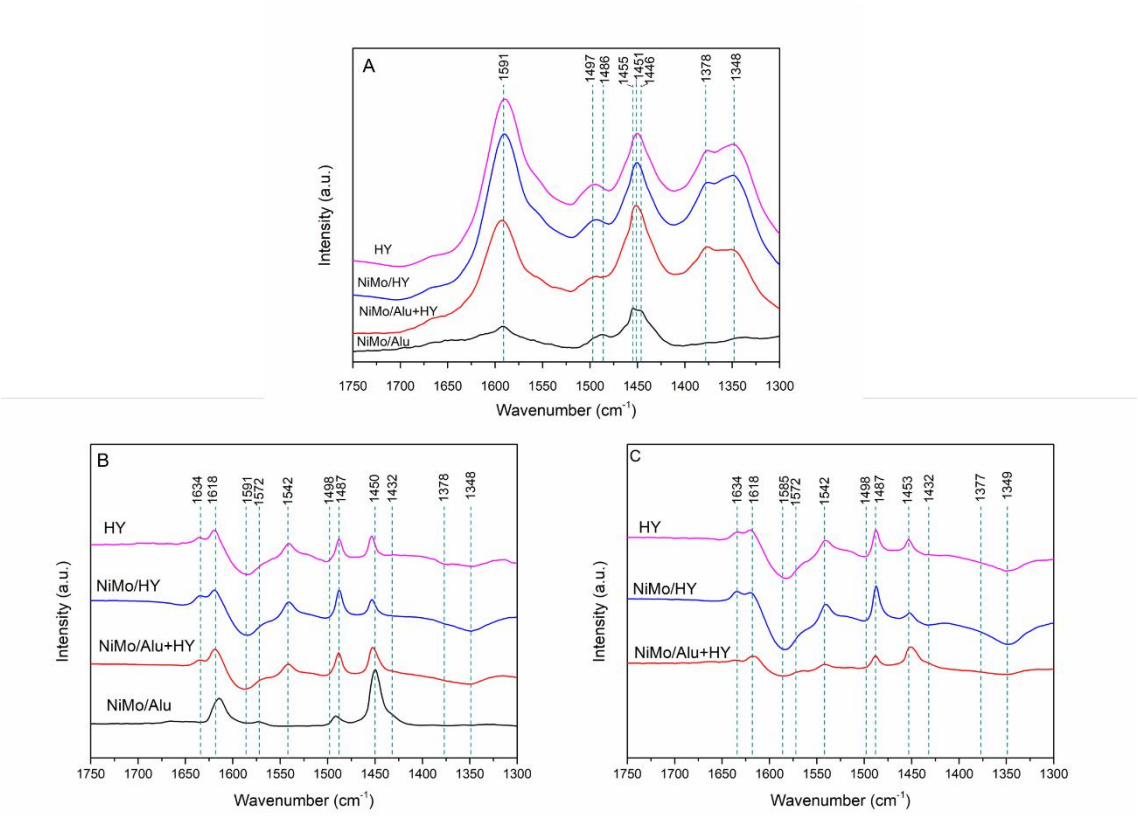

Figure 5. (A) Operando IR spectra of the sulfide catalysts taken after 10 minutes of reaction. (B) Spectral subtraction between the first spectra after and the last spectra before the first pyridine injection. (C) Spectral subtraction between the first spectra after and the last spectra before the second pyridine injection.

3.3.1. Cyclohexene conversion and coke formation

Figure 6A reports the coke evolution measured by the band at 1591 cm^{-1} (area per gram of zeolite on zeolite-containing materials and area per gram of alumina on NiMo/Alu) and cyclohexene conversion versus TOS for the various catalysts. All the zeolitic materials present intense deactivation as well as strong coke formation in the first 0.5 hour on stream (TOS).

Activity, as well as coke formation, further stabilize up to the first pyridine injection. By contrast, NiMo/Alu that presents the lowest activity does not exhibit any deactivation in agreement with its very low coke formation, which remains constant.

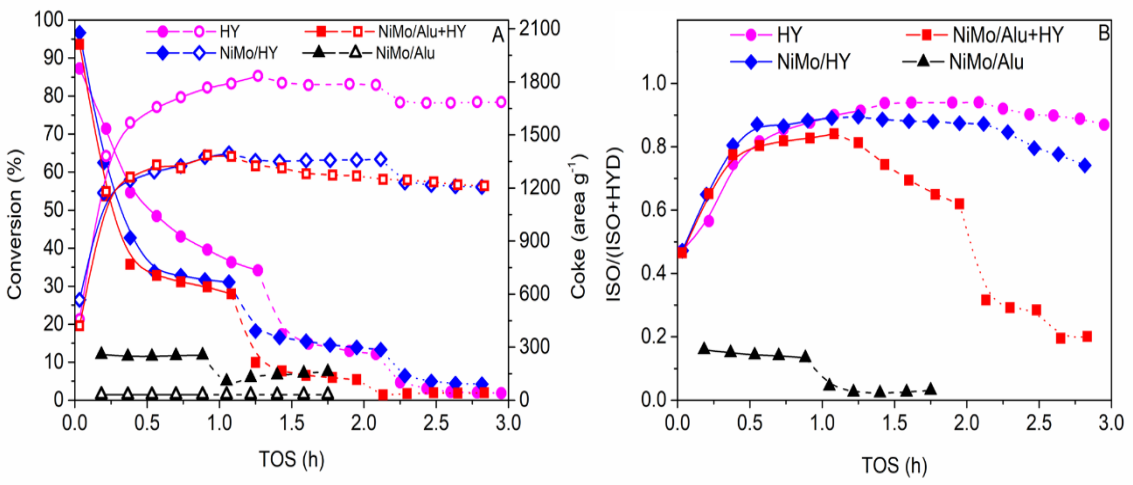

Figure 6. Operando IR/GC study of the various catalysts (A): Cyclohexene conversion (filled symbols, left axis) and coke formation (open symbols, right axis) and (B): isomerization/(isomerization + hydrogenation) ratio. Continuous lines: no pyridine addition; dashed lines: after first pyridine addition; dotted lines: after second pyridine addition. (There are small variations between the time of injection of the pyridine dose for the different catalysts).

The variation of coke band shown in Figure 6A evidences a start of stabilization of coking process after approximately 0.5 h of reaction. HY presents the highest coke deposition, while NiMo/HY and NiMo/Alu+HY show a similar amount. This means that the presence of the sulfide phase reduces coke formation. Nevertheless, the similar magnitudes of coke evolution exhibited by NiMo/HY and NiMo/Alu+HY during the tests suggest that the sulfide phase location does not affect coking process. However, it was expected that the catalyst with close proximity between zeolite and sulfide phase (NiMo/HY) presented less coke deposition than

NiMo/Alu+HY. Figure 6B points out the ISO/(ISO+HYD), calculated as the ratio between the yields of isomerization (1-methyl-1-cyclopentene and metylcyclopentane) and isomerization + hydrogenation (cyclohexane and methylcyclopentane) products. During the first hour of time-on-stream (TOS), NiMo/Alu+HY exhibits a lower value of this ratio than NiMo/HY i.e. higher hydrogenation activity. Thus, the reduced formation of coke on NiMo/Alu+HY could be associated with its increased hydrogenation activity despite the less proximity between both sites, resulting in coke deposition comparable to the catalyst with close proximity between both functions i.e. NiMo/HY.

3.3.2. Acid sites poisoning by pyridine pulse

The effects of acidic sites poisoning on the catalytic performances were studied. After about 1 h of reaction, a small dose of pyridine was injected on catalysts. Spectral subtraction between the first point after and the last point before such addition, displayed in Figure 5B (Spectra used for such subtractions are shown in Figures S4-S7), show the appearance of pyridine bands interacting with LAS at 1450 and 1618 cm^{-1} and BAS at 1542 and 1634 cm^{-1} [35], indicating a poisoning of acidic sites after pyridine addition. Figures 7 to 9 show that pyridine adsorption immediately impacted cyclohexene conversion and product yields and their variations with TOS, while coke amount on the catalysts presented a tiny decrease. The variation of BAS and LAS poisoned by pyridine versus TOS is reported in Figures 7B to 9B on zeolite-containing catalysts and Figure 10 on NiMo/Alu. Pyridine poisons both BAS and LAS on the zeolite-containing catalysts, but their variation with TOS is different. While the amount of BAS poisoned by pyridine slightly increases with TOS, the amount of poisoned LAS is maximum just after pyridine injection and then decreases up to a plateau. On NiMo/Alu, where no BAS is detected, the poisoned LAS variation with TOS follows a similar trend than on zeolite-containing catalysts, and recovery of cyclohexene conversion is noted in parallel to values close to those measured before the addition of pyridine. These changes indicate that LAS of different

strengths are present on the catalysts, whereas only the stronger ones remain poisoned for longer TOS. Indeed, alumina support and extra-framework phase of the zeolite possess Al^{3+} coordinatively unsaturated sites (CUS) with strong acidity, whereas sulfide phase presents CUS with weak acidity [44]. These results show that NiMoS sites are gradually released from pyridine poisoning, while Al^{3+} CUS sites are still poisoned. Progressive increase of BAS poisoning with TOS likely indicates that the pyridine released by weak LAS is re-adsorbed on BAS.

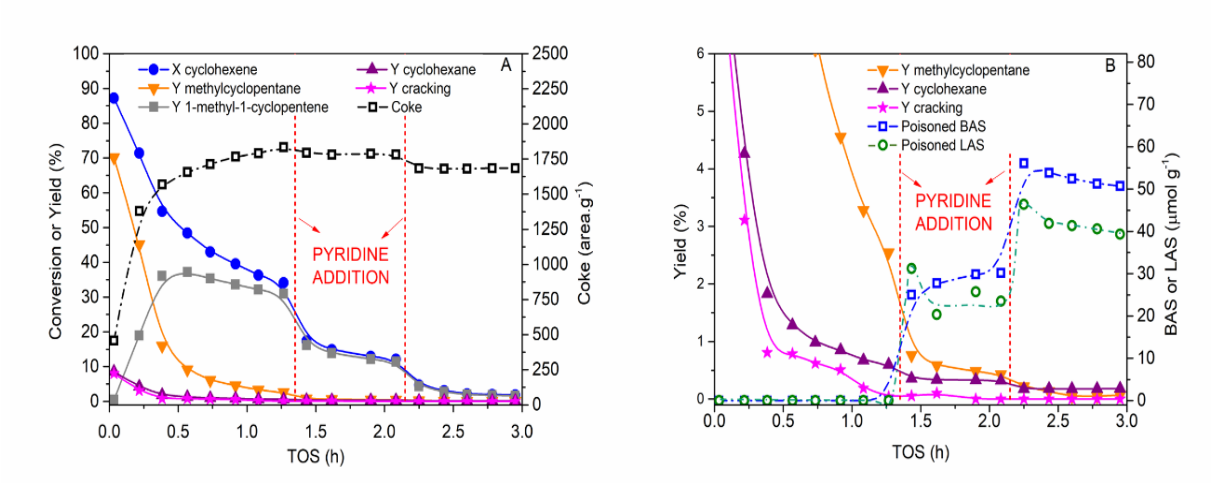

Figure 7. Operando IR/GC study of HY zeolite. (A): Cyclohexene conversion, product yields and coke deposition; (B): Poisoned BAS and LAS and amplified scale of catalytic data shown in (A) for better visualization.

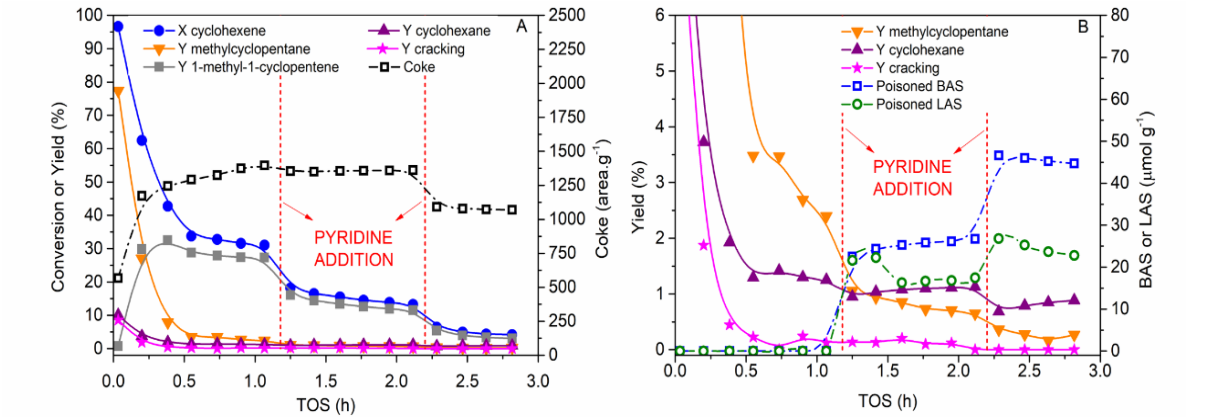

Figure 8. Operando IR/GC study of sulfide NiMo/HY catalyst. (A): Cyclohexene conversion, product yields, and coke deposition; (B): Poisoned BAS and LAS and amplified scale of catalytic data shown in (A) for better visualization.

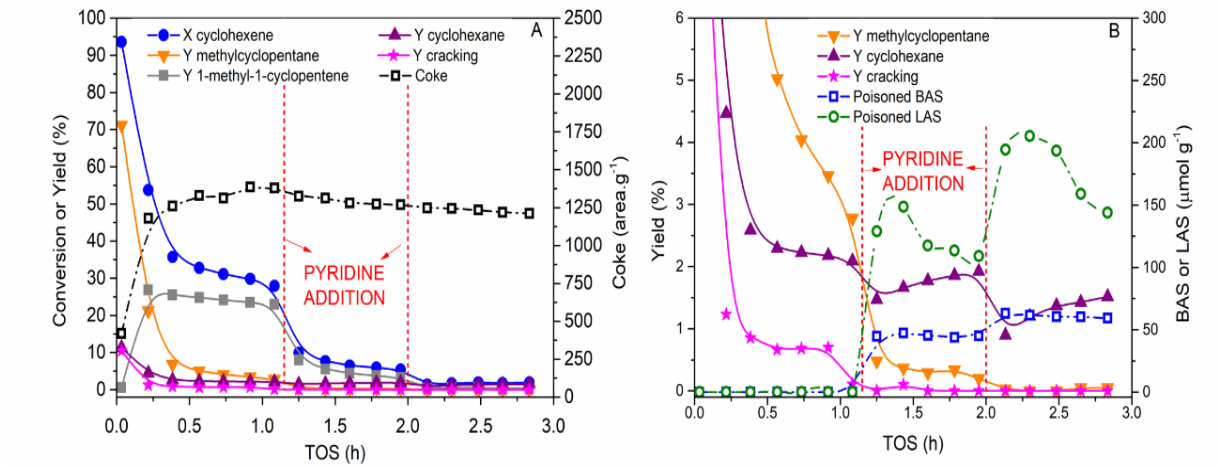

Figure 9. Operando IR/GC study of sulfide NiMo/Alu+HY catalyst. (A): Cyclohexene conversion, product yield, and coke deposition; (B): Poisoned BAS and LAS and amplified scale of catalytic data shown on (A) for better visualization.

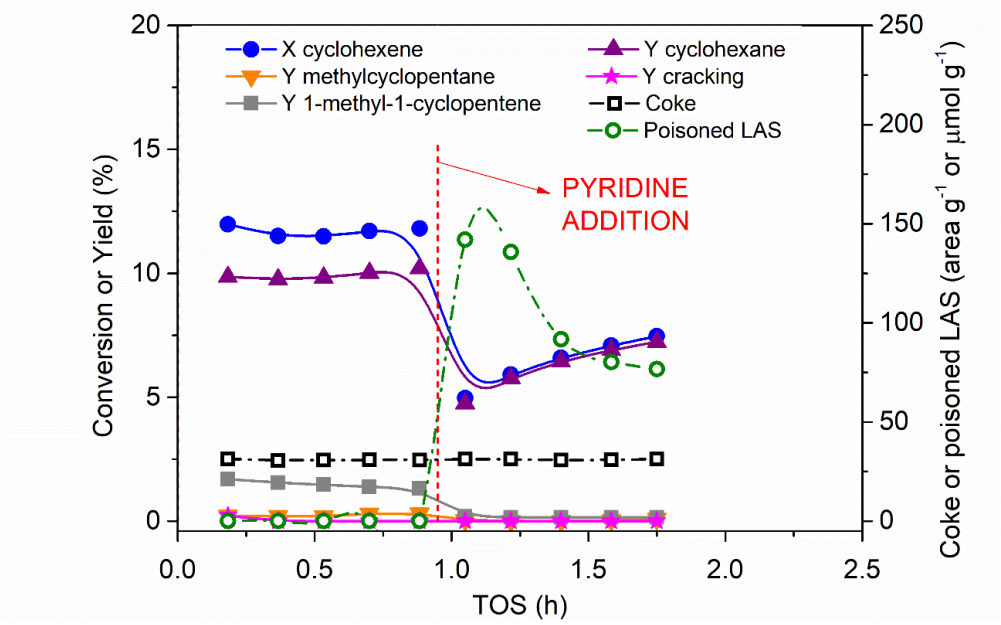

Figure 10. Operando IR/GC study of sulfide NiMo/Alu catalyst (cyclohexene conversion, products yield, coke deposition and poisoned LAS).

After about 2 h of reaction, the second dose of pyridine was injected on the zeolite-containing catalysts. Spectral subtractions between the first point after and the last point before such dose is shown in Figure 5C (Spectra used for such subtractions are shown in Figures S8 to S10), and similar behavior to the one of the first addition is observed, indicating an additional poisoning of acidic sites. Comparing the first point after and the last point before the first pyridine addition on all zeolite-containing samples in Figure 6A, NiMo/HY showed the lowest decrease of conversion after such dose, which suggests that the close proximity between acidic and sulfide sites exhibited by this catalyst promotes a higher resistance to nitrogen species. As observed after the first dose, a release of some weak LAS from sulfide phase initially poisoned is noted on NiMo/HY and NiMo/Alu+HY catalyst (Figures 8B and 9B).

3.3.3. Product yield and selectivity changes with TOS

The initial deactivation period observed on all the zeolite-containing catalysts markedly impacts the various product yields (Figures 7 to 9). A notable decrease in methylcyclopentane formation is observed. In parallel, an increase in 1-methyl-1-cyclopentene occurs. Then, after reaching a maximum of 1-methyl-1-cyclopentene formation, a lower deactivation rate was observed for all the reaction products, combined with a lower coke increase. On all the zeolite-containing catalysts, 1-methyl-1-cyclopentene and methylcyclopentane are the main reaction products. However, cyclohexane and cracking products are strongly affected by deactivation, and their yields become very small after a strong deactivation stage (0.5 h of TOS). NiMo/Alu catalyst did not present any remarkable initial deactivation, and cyclohexane is the main reaction product, which remains stable with TOS.

The initial deactivation has a remarkable effect on ISO/(ISO+HYD) ratio, ~~calculated as the ratio between the yields of isomerization (1-methyl-1-cyclopentene and metylcyclopentane) and isomerization + hydrogenation (cyclohexane and methylcyclopentane) products~~ as shown in Figure 6B. During the first 0.5 h on stream, this ratio continuously increases in all zeolitic catalysts due to the increase of 1-methyl-1-cyclopentene and decrease of the other products. Then, a stabilization of the ratio occurs in all catalysts with the decrease of the 1-methyl-1-cyclopentene yield. After 1 h of TOS, HY presented the highest ratio, followed by NiMo/HY and NiMo/Alu+HY. The NiMo/Alu catalyst presents a very low ISO/(ISO+HYD) ratio compared to the zeolitic ones, and this ratio remains constant with TOS. Analyzing the period before pyridine addition in Figure 10, the very low ratio is associated with the main formation of cyclohexane on NiMo/Alu. In addition, there is no variation on conversion and product formation with TOS, which means that no deactivation is observed for any reaction and, consequently, unchanged ISO/(ISO+HYD) ratio for this catalyst.

Figure 6A shows that pyridine injection for all the catalysts strongly decreases the cyclohexene conversion while the coke amount remains stable or slightly decreased. On the NiMo zeolitic catalysts, pyridine strongly decreases the 1-methyl-1-cyclopentene as well as methylcyclopentane yield, although cyclohexane yield is only slightly affected (Figures 8 and 9). Consequently, pyridine addition on NiMo catalyst leads to a decrease of the ISO/(ISO+HYD) ratio (Figure 6B). In contrast, HY presents a stabilization of ISO/(ISO+HYD) ratio after pyridine poisoning. After second pyridine poisoning, there is another decrease in cyclohexene conversion, and similar behavior to the one of the first pyridine addition regarding coke formation and product formation is noted in all catalysts. ISO/(ISO+HYD) ratio presents a substantial decrease in all catalysts, and the final value on NiMo/Alu+HY is rather close to that observed on NiMo/Alu catalyst.

3.3.4. Role of sulfide and acidic sites on reaction steps

On NiMo/Alu, cyclohexane is the main product; its yield decreases after pyridine introduction but increases again up to a value rather close to that measured before pyridine pulse after about one hour of TOS (Figure 10). In parallel, a fraction of the LAS poisoned by pyridine is recovered. This indicates that, on NiMo/Alu, LAS are involved in the hydrogenation reaction. A close inspection of the Figures 8B and 9B shows that, on NiMo/HY and NiMo/Alu+HY, cyclohexane yield decreases after pyridine introduction but afterward reaches a value close to that measured before pyridine pulse. Similarly, for these two catalysts, a recovering of a fraction of the poisoned LAS is observed with TOS. As already mentioned in the previous section, pyridine is removed from the weakest sites with TOS. This also shows that when pyridine is released from the weaker LAS of the NiMo catalysts, hydrogenation activity is recovered. The relationship between the release of weak CUS and the improved hydrogenation activity in NiMo/HY, NiMo/Alu+HY, and NiMo/Alu points out the participation of the sulfide sites in the formation of hydrogenation products.

It should be mentioned that this hydrogenation product can be formed by another route since pure HY zeolite also leads to the cyclohexane formation. In a previous paper, we have shown the involvement of the strongest acid OH group of HY zeolite in cyclohexane formation, although in a lower extent, through a hydrogen transfer mechanism [45]. Hence on the bifunctional sulfide catalysts, both strongly acidic zeolitic OH groups and sulfide CUS contribute to the formation of hydrogen transfer and hydrogenation steps, respectively. Note that strongly acidic zeolitic OH groups are rapidly poisoned by coke formed at the beginning of the reaction. Thus, only sulfide CUS are active for hydrogenation at longer TOS.

On pure HY zeolite, our previous paper shows [45] that medium acidic OH (OH groups at hexagonal prism and in sodalite cage) and weak acidic OH (SiOH) are responsible for the isomerization steps of cyclohexene reaction. The results obtained on zeolite-containing NiMo catalysts confirm this conclusion. Indeed, their product yield profiles with TOS are close to

those obtained on the parent zeolite. When rapid coke is formed at the first stage of TOS, 1-methyl-1-cyclopentene yield increases while methylcyclopentane and cyclohexane yields decrease due to the specific poisoning by rapid coking of the most acidic zeolitic OH groups and decreasing the contribution of hydrogen transfer reaction. At greater TOS, the yield of 1-methyl-1-cyclopentene starts to be affected. The further injection of pyridine that poisoned a significant fraction of available BAS, markedly decreases the 1-methyl-1-cyclopentene yield. All these results agree with the involvement of medium acidic zeolitic OH groups in the isomerization activity.

3.3.5 Turnover frequency (TOF) calculations

In the literature, only a few papers present turnover frequency (TOF) values for hydrogenation and isomerization of cyclic compounds. Moreover, the presented values are often questionable since activity per site, is in most of the cases, calculated considering the whole amount of active component present in the catalyst and not only the accessible species [46,47]. Besides, if dispersion is considered, it is generally the exposed sites of the freshly activated catalysts that are taken into consideration, and site coking or sintering during the reaction are generally not considered in the calculations. In contrast, the operando setup can allow interesting monitoring of the active sites and activity variations throughout the TOS [26,45,46]. Thus, as previously described, the introduction of pyridine pulse in the operando IR/GC set up allows to accounting simultaneously for the surface site poisoning and the catalyst performance changes. The previous results showed that the pyridine pulse modifies the BAS and LAS availability and impacts isomerization and hydrogenation activities. However, the question that arises is: do all the acidic sites poisons, or only a fraction of them are active for the considered route? In this way, very interesting are the changes that occur further with TOS after the pyridine pulse. Indeed, a fraction of LAS is reclaimed with TOS, giving rise to a recovery of hydrogenation activity. Moreover, it is observed that supplementary BAS are poisoned with TOS that leads to a

decrease in isomerization activity. Hence, from the parallel between the decrease in the amount of BAS and increase in LAS available, and the changes in the rate of formation of 1-methyl-1-cyclopentene and cyclohexane after the first pyridine dose, TOF can be calculated for isomerization and hydrogenation routes. Methylcyclopentane was not considered because its formation depends on 1-methyl-1-cyclopentene yield, and it is formed in very low concentration compared to parent olefin yield. Firstly, the rates were calculated considering pseudo-first-order reactions as described in the supplementary material (section D). Then, the variation of isomerization and hydrogenation reaction rates were calculated as shown in Equation (1), where Δr is the variation of the reaction rate (isomerization or hydrogenation), r_i is the reaction rate at a specific time, and r_{ref} is the rate at reference time.

$$\Delta r = r_i - r_{ref} \quad (1)$$

Variation of poisoned BAS and LAS were calculated according to Equation (2), where S_i is the concentration of poisoned sites (BAS or LAS) at a specific time and S_{ref} is the concentration of poisoned sites (BAS or LAS) at the reference time.

$$\Delta S = S_i - S_{ref} \quad (2)$$

TOF was calculated, as shown in Equation (3), where ISO and HYD refer to isomerization and hydrogenation reactions, respectively.

$$TOF_{iso} = \left|\frac{\Delta r_{iso}}{\Delta BAS}\right| \quad \text{and} \quad TOF_{hyd} = \left|\frac{\Delta r_{hyd}}{\Delta BAS + \Delta LAS}\right| \quad (3)$$

The value obtained by Equation (3) refers to the variation of reaction rate (isomerization or hydrogenation) with the variation of acidic sites amount after the first pyridine addition. At this stage, coke amount is constant in all catalysts, and the variation of poisoned sites can only be ascribed to pyridine adsorption.

As discussed in section 3.3.2 and shown in Figures 7 to 9 after pyridine pulse, poisoned BAS increases continuously with TOS in all catalysts, while 1-methyl-1-cyclopentene yield decreases

after the first pyridine addition. Thus, the first point after pyridine pulse was used as reference for applying Equations (1) and (2) and used for TOF calculations of the isomerization step. The values reported in Table 2 correspond to the average of TOF obtained by Equation (3) for the various TOS, and the uncertainties of the measures are shown in parenthesis.

In contrast, poisoned LAS achieve a maximum value on the first or second point measured after the pyridine pulse. Then, a strong decrease of poisoned sites is noted, which was associated in section 3.3.2 with the release of sulfide sites. In parallel, a decrease in cyclohexane formation is observed on the first sampling after pyridine pulse, and then its yield increases at the subsequent TOS (Figures 8 to 10). As previously, the first point (or second) after pyridine pulse was used as reference for applying Equations (1) and (2) and used for TOF determination of hydrogenation step by Equation (3) for the various TOS, whose average values and uncertainties (in parenthesis) are shown in Table 2.

The intrinsic activity for isomerization and hydrogenation are reported in Table 2. For all the catalysts, the TOF values for isomerization (1.2-1.9 10^{-1} s^{-1}) is greater by approximately one order of magnitude than the TOF values for hydrogenation (1.8-3.2 10^{-2} s^{-1}). This indicated that the poisoning effect of one pyridine molecule will be 10 times stronger on isomerization than on hydrogenation, evidencing the more toxic pyridine impact on isomerization activity. Table 3 summarizes TOF values reported in the literature, whose objective is to obtain an approximate comparison between the order of magnitude of the values calculated in this work and the ones reported by other works despite the differences of TOF determination. For hydrogenation reactions, it is highlighted that the values are greater of one order of magnitude than those calculated in the present work. Indeed, this is true for cyclohexene hydrogenation on CoMo/$MgAl_2O_3$ [48] and Pt/(Al_2O_3) [49], and the same occurs when comparing the values found for NiMo/HY and NiMo/Alu+HY and other zeolite-containing catalysts for tetralin hydrogenation such as NiW/USY [50] and Pt/HY [51]. Such differences are obviously ascribed to the fact that the exposed sites of the freshly activated catalysts are considered active, which

results in an underestimated TOF, but also to the more severe conditions of reaction that make the catalysts more active.

Regarding cyclohexene isomerization, to our knowledge, no TOF calculations are presented in the literature for this molecule or other cyclic compounds (such as tetralin and decalin). Nevertheless, a value for tetralin hydrocracking activity (which required medium-acidic BAS as isomerization) is reported by Sato *et al.* for NiW/USY [50], which is close to the ones found in this work.

Table 2. TOF calculated for isomerization route (1-methyl-1-cyclopentene) and hydrogenation route (cyclohexane) of cyclohexene hydroconversion reaction performed at 523 K and atmospheric pressure for the different catalysts.

Catalyst	TOF (s^{-1})	
	Isomerization	Hydrogenation
HY	1.2 (±0.1) x 10^{-1}	
NiMo/HY	1.5 (±0.1) x 10^{-1}	5.2 (±0.3) x 10^{-2}
NiMo/Alu+HY	1.9 (±0.7) x 10^{-1}	1.9 (±0.1) x 10^{-2}
NiMo/Alu		1.8 (±0.1) x 10^{-2}

Table 3. TOF values reported in the literature for reactions performed on sulfide/metallic sites (hydrogenation) and acidic sites (hydrocracking) as well as the experimental conditions used in the experiments.

		Hydrogenation of cyclic compounds				
Catalyst	TOF (s^{-1})	Reactant	P (bar)	T (K)	Active phase	Ref.

					measurement	
$CoMo/MgAl_2O_3$	1.6 x 10^{-1}	Cyclohexene	20	573	CO IR	[48]
Pt/Al_2O_3	102	Cyclohexene	1	323	H_2 chemisorption	[49]
NiW/USY	4.1 x 10^{-1}	Tetralin	60	573	NO chemisorption	[50]
Pt/HY	3 x 10^{-1}	Tetralin	60	623	H_2 chemisorption	[51]
		Hydrocracking of tetralin to monocyclic compounds				
NiW/USY	1.2 x 10^{-1}	Tetralin	60	573	NH_3 TPD	[50]

3.3.6. Effects of sulfide location on hydrogenation products

Hydrogenated products from cyclohexene can be formed by two routes on bifunctional catalysts, as shown in Figure 1. The first one is the direct cyclohexene hydrogenation to cyclohexane. In the second route, cyclohexene is firstly isomerized to 1-methyl-1-cyclopentene and then hydrogenated to methylcyclopentane.

Firstly, to study the effect of sulfide phase location on the hydrogenation activity, the impact of coke on hydrogenation was studied, and only cyclohexane production was considered. Figure 11 reports the variation of coke/cyclohexane ratios with TOS. This ratio is very low for NiMo/Alu in agreement with the limited amount of coke formed, whereas it is high for pure HY since in the absence of sulfide phase, the hydrogenation activity of the catalyst is low. More interesting are the different coke/cyclohexane ratios for NiMo/Alu+HY than for NiMo/HY, whereas the coke formation is equivalent to these two catalysts (Figure 6A). The lower coke/cyclohexane ratio on NiMo/Alu+HY evidences that coke is less toxic toward hydrogenation activity when NiMo phase is located on alumina than on zeolite. This indicates that, on NiMo/HY, the coke deposed on zeolite phase may block the accessibility to some

sulfide sites due to their close proximity, which decreases hydrogenation activity. On the other hand, such poisoning does not occur (or it exists in lower extension) on NiMo/Alu+HY, as the sulfide site is on alumina phase, which has low coke deposition and resulting in higher hydrogenation activity.

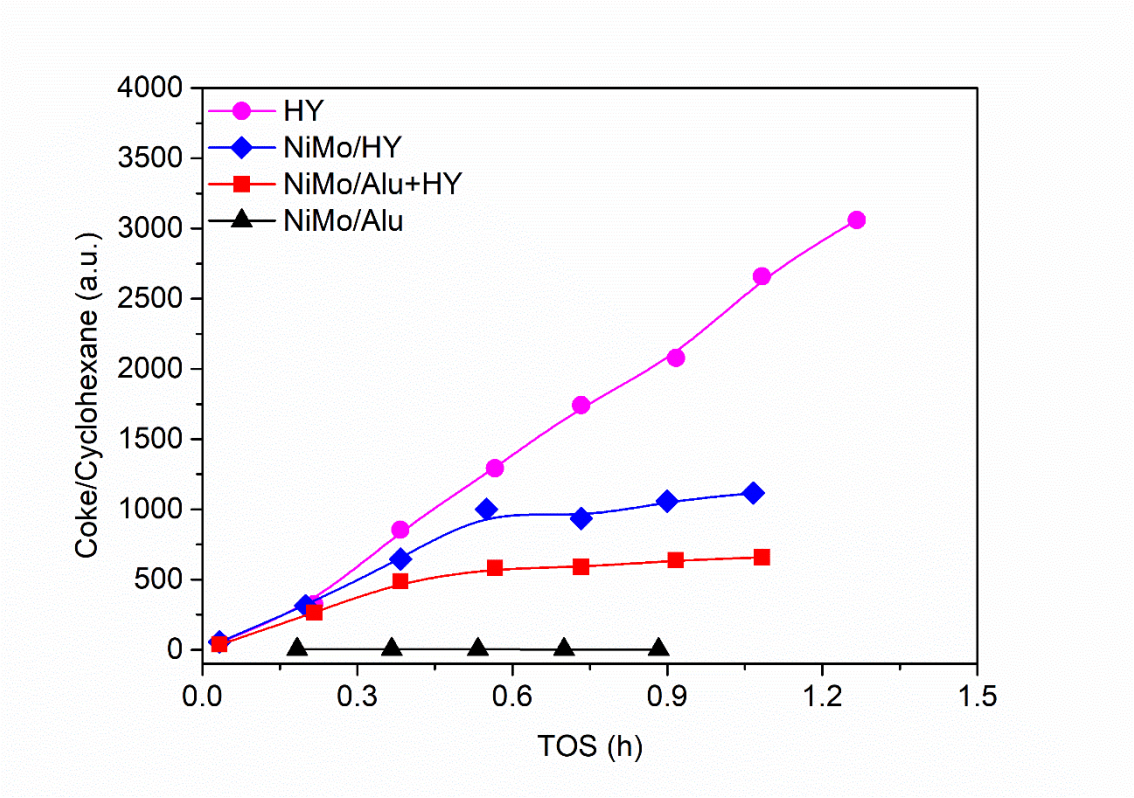

Figure 11. Coke/cyclohexane ratio measured at the period before the first pyridine addition.

Further was studied the impact of sulfide phase on the formation of the two hydrogenation products. Table 4 reports the cyclohexane and methylcyclopentane yields in three different periods on stream (before pyridine addition, after first, and after second pyridine doses). In the absence of pyridine, NiMo/Alu+HY exhibits higher yields of both products than NiMo/HY. As discussed previously, such behavior may be associated with lower coke toxicity when there is less proximity between sulfide and zeolitic sites. Regarding cyclohexane yield, it is expected an equivalent formation on NiMo/Alu+HY and NiMo/Alu catalysts, as the NiMo phase is on

alumina on both catalysts and coke deposition mainly occurs on zeolite phase. However, the first one exhibits lower formation of this product than the catalyst supported on pure alumina. Such behavior suggests a competition between zeolitic acid sites and sulfide phase for the reactant on NiMo/Alu+HY, which affects the reactant's distribution on the sites and consequently on product yield. Besides, NiMo/Alu catalyst presents only one hydrogenation product (cyclohexane), while NiMo/Alu+HY exhibits two hydrogenation products (methylcyclopentane and cyclohexane), resulting in a competition between the two hydrogenation routes for sulfide sites.

After first pyridine poisoning, the ISO/(ISO+HYD) ratio decrease is more intense for NiMo/Alu+HY than NiMo/HY (Figure 6B). First, this is related to a greater amount of BAS poisoned on NiMo/Alu+HY (45 $\mu mol.g^{-1}$) than on NiMo/HY (25 $\mu mol.g^{-1}$), which results in lower isomerization (ISO) activity by the first one. Second, this is related to the overall hydrogenation (HYD) activity higher on NiMo/Alu+HY than on NiMo/HY, mainly associated with the higher cyclohexane yield on NiMo/Alu+HY after the first pyridine dose (Table 4). This result shows that the direct hydrogenation activity is less affected by pyridine poisoning on NiMo/Alu+HY after first pyridine poisoning. As sulfide and acid sites are in separated domains, pyridine species are preferentially adsorbed on zeolite, and the sulfide sites on alumina would be more preserved. On NiMo/HY, pyridine is also preferentially adsorbed on zeolite, but such poisoning affects both sites, either because they are in close domains or by other mechanisms.

For example, acid sites may promote the hydrogenation activity of sulfides inside zeolite cages, and the poisoning of such sites reduces the promoting effect. Nevertheless, an interesting point to note in Table 4 is that methylcyclopentane yield is higher on NiMo/HY than NiMo/Alu+HY. This product is formed by sequential reactions, first isomerization (1-methyl-1-cyclopentene) and then hydrogenation, and the higher formation of methylcyclopentane is mainly associated with the higher yield of isomerization product on the first catalyst (Figures 8A and 9A).

After the second pyridine dose, the decrease of ISO/(ISO+HYD) ratio, as well as methylcyclopentane and cyclohexane formation, follow a similar trend than the previous dose on both catalysts. However, the whole amount of poisoned BAS is not so different from the previous dose (63 μmol.g^{-1} for NiMo/Alu+HY and 53 μmol.g^{-1} for NiMo/HY), which allows a better comparison between pyridine poisoning and catalytic behavior. The ISO/(ISO+HYD) ratio of NiMo/Alu+HY is close to NiMo/Alu at the end of the test (Figure 6B) i.e. very low isomerization activity and main formation of cyclohexane. On the other hand, NiMo/HY presents a higher formation of methylcyclopentane. Such results reveal that despite of the lower hydrogenation activity after pyridine doses, the higher resistance toward pyridine poisoning (regarding overall activity) promoted by the close proximity between acid and sulfide sites allows higher hydrogenation of the isomerized product formed on acid sites. Previous works [1,6] reported that methylcyclopentenes are intermediates for ring-opening reactions, and the fast hydrogenation (by sulfide sites) of the ring-opened product (on acid sites) is essential to minimize undesirable cracking products. As mentioned before, the results show that the close proximity between acid and sulfide sites allows a higher degree of hydrogenation of the isomerization product formed on acid sites, suggesting that the higher proximity has a beneficial effect for such route on bifunctional catalysts.

Table 4. Hydrogenation product yield exhibited by NiMo/HY and NiMo/Alu+HY catalysts at the end of first and second pyridine doses.

	Before pyridine addition		1st pyridine dose		2nd pyridine dose	
Catalyst	NiMo/ HY	NiMo/ Alu+HY	NiMo/ HY	NiMo/ Alu+HY	NiMo/ HY	NiMo/ Alu+HY
TOS (h)	1.1	1.1	2.1	2.0	2.8	2.8
Methylcyclopentane (mol %)	2.40	2.78	0.65	0.20	0.27	0.05
Cyclohexane (mol	1.25	2.09	1.13	1.92	0.88	1.52

%)						
Methylcyclopentane/cyclohexane ratio	1.92	1.33	0.57	0.10	0.31	0.03

4. Conclusions

The effects of the sulfide phase location in bifunctional catalysts on cyclohexene conversion were investigated. CO/IR spectra evidences the different locations of sulfide sites on NiMo/HY and NiMo/Alu+HY catalysts. Operando results of cyclohexene conversion reveal that pure zeolite presents higher coke formation than NiMo/HY and NiMo/Alu+HY, and the sulfide phase location in zeolite-containing catalysts is indifferent regarding coking process. However, the coke formed on NiMo/Alu+HY is mainly deposed over zeolite phase. Pyridine pulse injection during operando tests allowed controlled site poisoning. They point out the implication of sulfide sites on the hydrogenation route, whereas zeolitic OH groups are involved on the isomerization one. TOF calculations reveal a ten-time greater intrinsic activity for isomerization than for hydrogenation. Consequently, this leads to a more significant effect of N-molecules poisoning on isomerization activity than on hydrogenation activity. Regarding the effect of sulfide phase location, the catalyst with closer proximity between acid and sulfide sites, i.e. NiMo/HY, shows greater residual cyclohexene conversion after pyridine poisoning than the one with lower proximity, i.e., NiMo/Alu+HY. This evidences an increase in pyridine resistance when dual sites are closer. On the other hand, the closer proximity between both sites results in higher blockage of sulfide phase by coke, exhibiting lower activity for all hydrogenation products than the catalyst with lower dual-site proximity. In the presence of pyridine, hydrogenation activity performed by NiMo/Alu+HY is close to NiMo/Alu catalyst, where the hydrogenation product is mostly cyclohexane. In contrast, the closer proximity between sites results in higher hydrogenation of the isomerized product, formed on acid sites, which is beneficial to minimize cracking in more severe conditions. Hence, the IR/GC operando study of

bifunctional sulfide catalysts provided valuable information on the effect of the nature, strength, and location of catalyst sites in the different cyclohexene decomposition routes.

Acknowledgments

The authors thank Dr. Philippe Bazin, Dr. Alexandre Vimont, and Yoann Levaque for their support in developing the operando setup and the implementation of the experiments. PETROBRAS is thanked for its support of this work.

Declaration of competing Interest

The authors declare that they have no known competing financial interests or personal relationships that could have appeared to influence the work reported in this paper.

References

[1] H. Du, C. Fairbridge, H. Yang, Z. Ring, The chemistry of selective ring-opening catalysts, Appl. Cat. A. 294 (2005) 1–21. https://doi.org/10.1016/j.apcata.2005.06.033.

[2] R. Santana, P. Do, M. Santikunaporn, W. Alvarez, J. Taylor, E. Sughrue, D. Resasco, Evaluation of different reaction strategies for the improvement of cetane number in diesel fuels, Fuel. 85 (2006) 643–656. https://doi.org/10.1016/j.fuel.2005.08.028.

[3] E.J.M. Hensen, J.A.R. Van Veen, Encapsulation of transition metal sulfides in faujasite zeolite for hydroprocessing applications, Catal. Today. 86 (2003) 87–109. https://doi.org/10.1016/S0920-5861(03)00406-1.

[4] S.G.A. Ferraz, F.M.Z. Zotin, L.R.R. Araujo, J.L. Zotin, Influence of support acidity of NiMoS catalysts in the activity for hydrogenation and hydrocracking of tetralin, Appl. Catal. A. 384 (2010) 51–57. https://doi.org/10.1016/j.apcata.2010.06.003.

[5] C.A.A. Monteiro, D. Costa, J.L. Zotin, D. Cardoso, Effect of metal–acid site balance on hydroconversion of decalin over Pt/Beta zeolite bifunctional catalysts, Fuel. 160 (2015) 71–79. https://doi.org/10.1016/j.fuel.2015.07.054.

[6] M.A. Arribas, P. Concepción, A. Martínez, The role of metal sites during the coupled hydrogenation and ring opening of tetralin on bifunctional Pt(Ir)/USY catalysts, Appl. Catal. A. 267 (2004) 111–119. https://doi.org/10.1016/j.apcata.2004.02.037.

[7] P.S.F. Mendes, J.M. Silva, M.F. Ribeiro, C. Bouchy, A. Daudin, Quantification of the available acid sites in the hydrocracking of nitrogen-containing feedstocks over USY shaped NiMo-catalysts, J. Ind. Eng. Chem. 71 (2019) 167–176. https://doi.org/10.1016/j.jiec.2018.11.019.

[8] A. Travert, F. Maugé, IR study of hydrotreating catalysts in working conditions: comparison of the acidity present on the sulfided phase and on the alumina support, in:

B. Delmon, G.F. Froment, P. Grange (Eds.), Hydrotreating Hydrocracking Oil Fractions, Elsevier, Amsterdam, 1999: pp. 269–277.

[9] S. Jolly, J. Saussey, L.C. Lavalley, N. Zanier, E. Benazzi, J.F. Joly, The effect of 2,6-dimethylpyridine poisoning on the activity in n-hexane cracking of dealuminated HY zeolites, Ber. Bunsenges. Phys. Chem. 97 (1993) 313–315.

[10] J.F. Joly, N.Zanier-Szydlowski, S. Colin, F. Raatz, J. Saussey, J.C. Lavalley, Infrared in situ characterization of HY zeolite acid sites during cyclohexene transformation, Catal. Today. 9 (1991) 31–38.

[11] Y. Zhang, D. Fu, X. Xu, Y. Sheng, J. Xu, Y.F. Han, Application of operando spectroscopy on catalytic reactions, Curr. Opin. Chem. Eng. 12 (2016) 1–7. https://doi.org/10.1016/j.coche.2016.01.004.

[12] A. Chakrabarti, M.E. Ford, D. Gregory, R. Hu, C.J. Keturakis, S. Lwin, Y. Tang, Z. Yang, M. Zhu, M.A. Bañares, I.E. Wachs, A decade+ of operando spectroscopy studies, Catal. Today. 283 (2017) 27–53. https://doi.org/10.1016/j.cattod.2016.12.012.

[13] H. Li, S.A. Kadam, A. Vimont, R.F. Wormsbecher, A. Travert, Monomolecular cracking rates of light alkanes over zeolites determined by IR operando spectroscopy, ACS Catal. 6 (2016) 4536–4548. https://doi.org/10.1021/acscatal.6b01025.

[14] S.A. Kadam, H. Li, R.F. Wormsbecher, A. Travert, Impact of zeolite structure on entropic–enthalpic contributions to alkane monomolecular cracking: an IR operando study, Chem. Eur. J. 24 (2018) 5489–5492. https://doi.org/10.1002/.

[15] M. Anand, S.A. Farooqui, J. Singh, H. Singh, A.K. Sinha, Mechanistic in-operando FT-IR studies for hydroprocessing of triglycerides, Catal. Today. 309 (2018) 11–17. https://doi.org/10.1016/j.cattod.2017.12.021.

[16] T. Lesage, C. Verrier, P. Bazin, J. Saussey, M. Daturi, Studying the NO_x-trap mechanism

over a Pt-Rh/Ba/Al_2O_3 catalyst by operando FT-IR spectroscopy, Phys. Chem. Chem. Phys. 5 (2003) 4435–4440. https://doi.org/10.1039/b305874n.

[17] A.K. Aboul-Gheit, S.M. Aboul-Fotouh, N.A.K. Aboul-Gheit, Effect of combining palladium, iridium or rhenium with platinum supported on H-ZSM-5 zeolite on their cyclohexene hydroconversion activities, Appl. Catal. A. 292 (2005) 144–153. https://doi.org/10.1016/j.apcata.2005.05.041.

[18] R. Romero-Rivera, M. Delvalle, G. Alonso, E. Flores, F. Castillon, S. Fuentes, J. Cruzreyes, Cyclohexene hydrogenation with molybdenum disulfide catalysts prepared by ex situ decomposition of ammonium thiomolybdate-cetyltrimethylammonium thiomolybdate mixtures, Catal. Today. 130 (2008) 354–360. https://doi.org/10.1016/j.cattod.2007.10.099.

[19] Z. Vít, D. Gulkova, L. Kaluza, M. Zdrazil, Synergetic effects of Pt and Ru added to Mo/AlO sulfide catalyst in simultaneous hydrodesulfurization of thiophene and hydrogenation of cyclohexene, J. Catal. 232 (2005) 447–455. https://doi.org/10.1016/j.jcat.2005.04.006.

[20] B.M. des Rochettes, C. Marcilly, G. Gueguen, J. Bousquet, Kinetic study of hydrogen transfer of olefins under catalytic cracking conditions, Appl. Catal. 58 (1990) 35–52.

[21] J. Dwyer, K. Karim, A.F. Ojo, Bimolecular hydrogen transfer over zeolites and SAPOs having the faujasite structure, J. Chem. Soc. Faraday Trans. 87 (1991) 783–796.

[22] S. Garg, K. Soni, T. Ajeeth Prabhu, K.S. Rama Rao, G. Murali Dhar, Effect of ordered mesoporous Zr SBA-15 support on catalytic functionalities of hydrotreating catalysts 2. Variation of molybdenum and promoter loadings, Catal. Today. 261 (2016) 128–136. https://doi.org/10.1016/j.cattod.2015.08.051.

[23] K.A. Bukin, O. V Potapenko, V.P. Doronin, T.P. Sorokina, T.I. Gulyaeva, Performance

of a zeolite-containing catalyst and catalysts based on noble metals in intermolecular hydrogen transfer between C6 hydrocarbons, Kinet. Catal. 58 (2017) 271–278. https://doi.org/10.1134/s002315841703003x.

[24] M. Boudart, C.M. McConica, Catalytic hydrogenation of cyclohexene, J. Catal. 117 (1989) 33–41.

[25] S. Jolly, J. Saussey, L.C. Lavalley, FT-IR study of hydrocarbon conversion on dealuminated HY zeolites in working conditions, J. Mol. Catal. 86 (1994) 401–421.

[26] T. Lesage, C. Verrier, P. Bazin, J. Saussey, M. Daturi, Studying the NO_x-trap mechanism over a Pt-Rh/Ba/Al_2O_3 catalyst by operando FT-IR spectroscopy, Phys. Chem. Chem. Phys. 5 (2003) 4435–4440. https://doi.org/10.1039/b305874n.

[27] S. Khabtou, T. Chevreau, J.C. Lavalley, Quantitative infrared study of the distinct acidic hydroxyl groups contained in modified Y zeolites, Micro. Mater. 3 (1994) 133–148.

[28] K. Hadjiivanov, Identification and characterization of surface hydroxyl groups by infrared spectroscopy, Adv. Catal. 57 (2014) 99–318. https://doi.org/10.1016/b978-0-12-800127-1.00002-3.

[29] F.A. Braggio, M.D. Mello, B.C. Magalhães, J.L. Zotin, M.A.P. Silva, Effect of pH on activity of NiMo/Al_2O_3 catalysts prepared with citric acid in simultaneous hydrodesulfurization and hydrodenitrogenation reactions, Catal. Lett. 147 (2017) 1104–1113. https://doi.org/10.1007/s10562-016-1903-6.

[30] J. Francis, E. Guillon, N. Bats, C. Pichon, A. Corma, L.J. Simon, Design of improved hydrocracking catalysts by increasing the proximity between acid and metallic sites, Appl. Catal. A. 409–410 (2011) 140–147. https://doi.org/10.1016/j.apcata.2011.09.040.

[31] C.E. Hédoire, E. Cadot, F. Villain, A. Davidson, C. Louis, M. Breysse, Preparation and characterization of molybdenum sulfide supported on β-zeolites obtained from

$[Mo_3S_4(H_2O)_9]^{4+}$ precursor, Appl. Catal. A. 306 (2006) 165–174. https://doi.org/10.1016/j.apcata.2006.03.045.

[32] C.-E. Hédoire, C. Louis, A. Davidson, M. Breysse, F. Maugé, M. Vrinat, Support effect in hydrotreating catalysts: hydrogenation properties of molybdenum sulfide supported on β-zeolites of various acidities, J. Catal. 220 (2003) 433–441. https://doi.org/10.1016/s0021-9517(03)00308-7.

[33] A. Travert, C. Dujardin, F. Maugé, E. Veilly, S. Cristol, J.-F. Paul, E. Payen, CO adsorption on CoMo and NiMo sulfide catalysts: a combined IR and DFT study, J. Phys. Chem B. 110 (2006) 1261–1270.

[34] A. Rocha, A. Farojr, L. Oliviero, J. Vangestel, F. Mauge, Alumina-, niobia-, and niobia/alumina-supported NiMoS catalysts: surface properties and activities in the hydrodesulfurization of thiophene and hydrodenitrogenation of 2,6-dimethylaniline, J. Catal. 252 (2007) 321–334. https://doi.org/10.1016/j.jcat.2007.09.012.

[35] F. Thibault-Starzyk, F. Maugé, Infrared spectroscopy, in: M. Che, J.C. Védrine (Eds.), Charact. Solid Mater. Heterog. Catal., Wiley-VCH Verlag GmbH & Co. KGaA, Weinheim, Germany, 2012: pp. 1–48. https://doi.org/10.1002/9783527645329.ch1.

[36] M. Breysse, P. Afanasiev, C. Geantet, M. Vrinat, Overview of support effects in hydrotreating catalysts, Catal. Today. 86 (2003) 5–16. https://doi.org/10.1016/S0920-5861(03)00400-0.

[37] A.S. Rocha, A.C. Faro, L. Oliviero, M.A. Lélias, A. Travert, J. Van Gestel, F. Maugé, Effect of the electronic properties of Mo sulfide phase on the hydrotreating activity of catalysts supported on Al_2O_3, Nb_2O_5 and Nb_2O_5/Al_2O_3, Catal. Lett. 111 (2006) 27–34. https://doi.org/10.1007/s10562-006-0126-7.

[38] J. Leglise, A. Janin, J.C. Lavalley, D. Cornet, Nickel and molybdenum sulfides loaded

into zeolites: activity for catalytic hydrogenation, J. Catal. 114 (1988) 388–397. https://doi.org/10.1016/0021-9517(88)90042-5.

[39] A.A. Gabrienko, I.G. Danilova, S.S. Arzumanov, L. V Pirutko, D. Freude, A.G. Stepanov, Direct measurement of zeolite Brønsted acidity by FTIR spectroscopy: solid-state ^{1}H MAS NMR approach for reliable determination of the integrated molar absorption coefficients, J. Phys. Chem. C. 122 (2018) 25386–25395. https://doi.org/10.1021/acs.jpcc.8b07429.

[40] N. Malicki, P. Beccat, P. Bourges, C. Fernandez, A.A. Quoineaud, L.J. Simon, F. Thibault-Starzyk, A new model for acid sites in dealuminated Y zeolites, Elsevier B.V., 2007. https://doi.org/10.1016/S0167-2991(07)80918-9.

[41] A. Vimont, F. Thibault-Starzyk, M. Daturi, Analysing and understanding the active site by IR spectroscopy, Chem.Soci. Rev. 39 (2010) 4928–4950. https://doi.org/10.1039/b919543m.

[42] J. Long, X. Wang, Z. Ding, L. Xie, Z. Zhang, J. Dong, H. Lin, Cyclopentadiene transformation over H-form zeolites : TPD and IR studies of the formation of a monomeric cyclopentenyl carbenium ion intermediate and its role in acid-catalyzed conversions, J. Catal. 255 (2008) 48–58. https://doi.org/10.1016/j.jcat.2008.01.023.

[43] B. Paweewan, P.J. Barrie, L.F. Gladden, Coking and deactivation during n-hexane cracking in ultrastable zeolite Y, Appl. Catal. A. 185 (1999) 259–268. https://doi.org/10.1016/S0926-860X(99)00143-X.

[44] G. Berhault, M. Lacroix, M. Breysse, F. Maugé, J.C. Lavalley, In situ characterization of transition metal sulfide catalysts by IR probe molecules adsorption and model reactions, Stud. Surf. Sci. Catal. 130 A (2000) 479–484. https://doi.org/10.1016/s0167-2991(00)81003-4.

[45] B.M. Santos, J.L. Zotin, F. Maugé, L. Oliviero, W. Zhao, M.A.P. da Silva, Strong and weakly acidic OH groups of HY zeolite into the different routes of cyclohexene reaction: an IR operando study, Catal. Lett. (2020). https://doi.org/10.1007/s10562-020-03424-4.

[46] M. El-Roz, P. Bazin, M. Daturi, F. Thibault-Starzyk, Operando infrared (IR) coupled to steady-state isotopic transient kinetic analysis (SSITKA) for photocatalysis: reactivity and mechanistic studies, ACS Catal. 3 (2013) 2790–2798. https://doi.org/10.1021/cs4006088.

[47] S. Kozuch, J.M.L. Martin, "Turning over" definitions in catalytic cycles, ACS Catal. 2 (2012) 2787–2794. https://doi.org/10.1021/cs3005264.

[48] T.L. Coelho, S. Arias, V.O. Rodrigues, S.S.X. Chiaro, L. Oliviero, F. Maugé, A.C. Faro Jr, Characterisation and performance of hydrotalcite-derived CoMo sulphide catalysts for selective HDS in the presence of olefin, Catal. Sci. Technol. 8 (2018) 6204–6216. https://doi.org/10.1039/c8cy01855c.

[49] Y.W. Chen, C. Li, Liquid phase hydrogenation of cyclohexene over Pt/aluminum borate catalyst, Catal. Lett. 13 (1992) 359–361. https://doi.org/10.1007/BF00765038.

[50] K. Sato, Y. Iwata, Y. Miki, H. Shimada, Hydrocracking of tetralin over NiW/USY zeolite catalysts: for the improvement of heavy-oil upgrading catalysts, J. Catal. 186 (1999) 45–56.

[51] D.E. Ramaker, J. de Graaf, D.C. Koningsberger, J.A.R. van Veen, Nature of the metal–support interaction in supported Pt catalysts: shift in Pt valence orbital energy and charge rearrangement, J. Catal. 203 (2001) 7–17. https://doi.org/10.1006/jcat.2001.3299.